# Universality of stringlet excitations as the origin of the boson peak of glasses with isotropic interactions

Yuan-Chao Hu [1] and Hajime Tanaka [1,2,*]

[1]*Department of Fundamental Engineering, Institute of Industrial Science, The University of Tokyo, 4-6-1 Komaba, Meguro-ku, Tokyo 153-8505, Japan*

[2]*Research Center for Advanced Science and Technology, The University of Tokyo, 4-6-1 Komaba, Meguro-ku, Tokyo 153-8904, Japan*

(Received 22 July 2022; accepted 22 March 2023; published 25 April 2023)

Nonphononic vibrations originating from disordered structures have garnered significant attention as a fundamental feature of glasses that distinguishes them from crystals. Recently, we discovered that one-dimensional (1D) stringlike vibrations without volume change are responsible for the boson peak in the reduced density of states of two-dimensional (2D) glasses [Y.-C. Hu and H. Tanaka, Nat. Phys. **18**, 669 (2022)]. Here we investigate the vibrational properties of three-dimensional (3D) model glasses with isotropic repulsive and attractive interactions and find that the boson peak arises from stringlike quasilocalized transverse vibrations in these 3D systems. These results suggest that stringlike vibrations are the universal origin of the boson peak in both 2D and 3D model glasses, as long as the interaction is isotropic. Furthermore, we confirm that the characteristic frequency of the quasilocalized transverse vibrations, i.e., the boson peak frequency, coincides with the Ioffe-Regel limit of transverse phonons. These results imply the boson peak originates from the frequency-resonant scattering of transverse phonons by quasilocalized vibrations rather than phonon scattering due to elastic inhomogeneity. Our findings provide insights into the origin of low-temperature glass anomalies and inspire further research.

DOI: 10.1103/PhysRevResearch.5.023055

## I. INTRODUCTION

Because of their disordered structures, glasses have vibrational properties distinct from crystals in which only coherent phonons are excited [1–3]. Despite the detailed structures of glasses being different among various systems, they commonly exhibit an excess vibrational density of states (VDOS) over the Debye prediction. The peak in the reduced VDOS, $D(\omega)/\omega^{d-1}$ ($d$: dimensionality) is widely known as the boson peak [3–8]. These peculiar low-frequency vibrational properties have been thought of as the origin of the universal low-temperature anomalies of the heat capacity and thermal conductivity in a similar energy scale [3,9,10]. Various theoretical models [11–25] have been proposed in the past several decades to explain the physical mechanism of the boson peak, but with controversies. The importance of quasilocalized modes (QLMs) has been pointed out by many researchers (e.g., [10,26–30]). One of the significant difficulties comes from the hybridization of QLMs with phonons, making isolating the relevant vibration modes challenging [10,31,32]. For example, the participation ratio (PR) has often been adopted to single out specific vibrational modes with a purely quasilocalized nature [33,34]. However, this strategy is effective only at a very low frequency below the first sound mode frequency in the system. At higher frequencies, especially around the boson peak frequency ($\omega_{\rm BP}$), QLMs significantly couple with phonons [9,10,26–30,35,36].

Another critical question is the roles of the transverse and longitudinal vibrational excitations in building up the boson peak. A clue has been provided by establishing a correlation between $\omega_{\rm BP}$ and the Ioffe-Regel limit of transverse phonons $\omega_{\rm IR}^{\rm T}$ convincingly [37]. However, this situation may depend on the type of interatomic interactions [38–41]. Beyond the universality, the relationship of the boson peak's nature with the materials' properties, such as the fragility and Poisson's ratio, has also been a matter of interest [42,43]. Decomposing the vibrational modes at a specific frequency in real space is essential to answer these questions.

We recently discovered that the boson peak originates from purely transverse stringlike vibrations for two-dimensional (2D) model glasses with isotropic potentials [36]. These stringlike vibrations, which may be a consequence of the hybridization of transverse phonons with QLMs [44–49], involve no volume change. We directly detected them in transverse dynamic structure factors $S_{\rm T}(q,\omega)$ ($q$: wave number) as a distinct $q$-independent peak around $\omega_{\rm BP}$, in the $q$ range above the transverse Ioffe-Regel limit wave number $q_{\rm IR}^{\rm T}$. Therefore, we concluded that the stringlike quasilocalized vibrations (QLVs) responsible for the boson peak are characterized by the unique energy (frequency) rather than the unique length [36,37]. Here we use the term QLV, which is hybridized with phonons, to distinguish it from QLM.

A significant question arises about the dimensionality's effect on the origin of the boson peak. How the glass

*tanaka@iis.u-tokyo.ac.jp

properties depend on dimensionality is one of the critical issues in glass research. For example, the Mermin-Wagner effects, long-wavelength fluctuations in 2D, strongly influence the slow motion of particles [50–52]. For crystals, the Debye theory has $d$ dependence. The spatial dimensionality is also critical theoretically since the fluctuation effects beyond the mean-field theory depend on the distance from the critical dimension [53–55]. More interestingly, the basic structure of multipolar (quadrupolar in 2D) QLMs critically depends on the dimension. They have different angular symmetry and the decay exponent of long-range stress ($r^{-d}$) between two and three dimensions [56–60]. The $d$ dependence of the low-frequency scaling laws of these QLMs is also a matter of debate [33,34,61]. Moreover, three-dimensional (3D) glasses are more relevant for understanding real-world glasses. These indicate the critical importance of revealing the origin of the boson peak in 3D glasses and its $d$ dependence.

## II. METHODS

### A. Computer simulations

We study two different binary glass models in three dimensions by molecular dynamics simulations. In all our simulations, periodic boundary conditions are imposed, and $NVT$ ensemble is employed. The reduced Lennard-Jones units are used throughout the simulation and analysis. Fifty independent simulations were performed for the ensemble average.

One glass model interacts via the inverse power-law potential model (3DIPL):

$$U_{\alpha\beta}(r) = \epsilon\left(\frac{\sigma_{\alpha\beta}}{r}\right)^{10}, \tag{1}$$

where we set $\sigma_{\rm AA} = 1.0$, $\sigma_{\rm BB} = 1.40$, and $\sigma_{\rm AB} = 1.18$ ($\alpha, \beta \in \{\rm A, B\}$) [62]. The composition is 50:50. All mass $m$ and the cohesive energy $\epsilon$ are set to 1.0. The potential and force are truncated and shifted to zero at $1.48\sigma_{\alpha\beta}$. We mainly study a cubic system with $N = 6750$ atoms with a number density of $\rho = 0.82$. The box length is $L_x = L_y = L_z = 20.19$. The glass transition temperature has been measured to be $T_{\rm g} = 0.50$ [62]. To obtain low-temperature glass states, we first melt and equilibrate the sample at high temperatures $T = 3.0$ and $T = 1.0$ for both $t = 4000$. Then the liquid is quenched to $T = 0.1$ at a cooling rate of $10^{-3}$. The corresponding inherent structures are achieved by the conjugate gradient algorithm, after relaxing the glassy solids for a period of $t = 2000$.

In addition to the above cubic system, we also study two other samples similarly (see the Appendix). One is cubic with $N = 1000$ atoms to consider the finite-size effect. The other is noncubic with $N = 6750$ and $L_x = 67.30$ while $L_y = L_z = 10.77$, so we can access lower frequency and lower wave number information.

The other glass model is the Kob-Andersen model (3DKA), in which the particles interact via

$$U_{\alpha\beta}(r) = 4\epsilon_{\alpha\beta}\left[\left(\frac{\sigma_{\alpha\beta}}{r}\right)^{12} - \left(\frac{\sigma_{\alpha\beta}}{r}\right)^{6}\right], \tag{2}$$

where $\alpha, \beta \in \{\rm A, B\}$, $\sigma_{\rm AA} = 1.0$, $\sigma_{\rm BB} = 0.88$, $\sigma_{\rm AB} = 0.8$, $\epsilon_{\rm AA} = 1.0$, $\epsilon_{\rm BB} = 0.5$, and $\epsilon_{\rm AB} = 1.5$ [63]. The potential and force are truncated and shifted at $r = 2.50\sigma_{\alpha\beta}$. The composition is 80:20. We study a cubic system with $N = 6750$ atoms with the number density of $\rho = 1.20$. The low-temperature glass solids at $T = 0.1$ and their corresponding inherent structures are obtained by a procedure similar to the above. Unlike the purely repulsive 3DIPL model, 3DKA includes long-range attractive interactions.

### B. Vibration analysis

We characterize the vibrational properties of the glasses by directly diagonalizing the Hessian matrix of the inherent structure [64–66]. No negative eigenvalue was found in any of our samples. The dynamical matrix is generally given by

$$D_{ij} = \frac{\partial^2 U}{\partial R_i \partial R_j}, \tag{3}$$

in which $R_i$ is the coordinate ($x$, $y$, or $z$) of particle $i$. The density of states is thus defined as

$$D(\omega) = \frac{1}{3N-3}\sum_{\lambda}\delta(\omega - \omega_\lambda). \tag{4}$$

The participation ratio (PR) [9] of a vibrational mode is measured by

$$\mathrm{PR} = \frac{\left(\sum_i^N |\vec{u}_i|^2\right)^2}{N\sum_i^N (\vec{u}_i \cdot \vec{u}_i)^2}. \tag{5}$$

### C. Dynamical structure factors

The transverse and longitudinal dynamical structure factors $S_{\rm T}(q,\omega)$ and $S_{\rm L}(q,\omega)$ are calculated from the above normal mode analysis [37]:

$$S_{\rm T}(q,\omega) = \frac{k_{\rm B}T}{M}\frac{q^2}{\omega^2}\sum_{\lambda} E_{\lambda,{\rm T}}(\mathbf{q})\delta(\omega-\omega_\lambda) \tag{6}$$

and

$$S_{\rm L}(q,\omega) = \frac{k_{\rm B}T}{M}\frac{q^2}{\omega^2}\sum_{\lambda} E_{\lambda,{\rm L}}(\mathbf{q})\delta(\omega-\omega_\lambda), \tag{7}$$

where for each mode λ

$$E_{\lambda,{\rm T}}(\mathbf{q}) = \left|\sum_j [\hat{\mathbf{q}}\times\vec{u}_j]\exp(i\mathbf{q}\cdot R_j)\right|^2 \tag{8}$$

and

$$E_{\lambda,{\rm L}}(\mathbf{q}) = \left|\sum_j [\hat{\mathbf{q}}\cdot\vec{u}_j]\exp(i\mathbf{q}\cdot R_j)\right|^2. \tag{9}$$

Here, $\hat{\mathbf{q}}$ is the unit wave vector, and $M$ is the particle effective mass. For cubic samples, the dynamical structure factors are averaged over different wave vectors with the same wave number. For the noncubic samples, only the wave vectors along the $x$ axis are considered.

### D. Vibrational mode decomposition

Each vibrational mode has been decomposed to the transverse and longitudinal components using a volume matrix

method [36,67]. A matrix $A$ is firstly built as

$$A_{i,j\alpha} = \frac{1}{V_i}\frac{\partial V_i}{\partial R_{j\alpha}}, \tag{10}$$

where $V_i$ is the local volume of particle $i$. Then an eigenvector $\vec{u}$ is projected to the transverse and longitudinal directions as $\vec{u}_{\rm L} = A^T(AA^T)^{-1}A\vec{u}$ and $\vec{u}_{\rm T} = \vec{u} - \vec{u}_{\rm L}$. The local volume is conserved for the transverse mode.

The vibrational density of states of transverse and longitudinal components are thus calculated by

$$D^{\rm T}(\omega) = \frac{1}{3N-3}\sum_{\lambda}\|\vec{u}_{\lambda,{\rm T}}\|^2\delta(\omega-\omega_\lambda) \tag{11}$$

and

$$D^{\rm L}(\omega) = \frac{1}{3N-3}\sum_{\lambda}\|\vec{u}_{\lambda,{\rm L}}\|^2\delta(\omega-\omega_\lambda). \tag{12}$$

We also calculate the atomic transverse VDOS defined as

$$D_i^{\rm T}(\omega) = \frac{1}{3N-3}\sum_{\lambda}\|\vec{u}_{\lambda,{\rm T}}(i)\|^2\delta(\omega-\omega_\lambda). \tag{13}$$

The sum of $D_i^{\rm T}(\omega)$ over all particles gives the transverse $D(\omega)$. Then, we calculate the intensity of the reduced VDOS for particle $i$ at $\omega_x$, $D_i^{\rm T}(\omega_x)/\omega_x$, as

$$D_i^{\rm T}(\omega_x)/\omega_x = \frac{1}{2\omega_x\Delta\omega}\int_{\omega_x-\Delta\omega}^{\omega_x+\Delta\omega} D_i^{\rm T}(\omega')d\omega'. \tag{14}$$

We choose $\Delta\omega = 0.2$ in this study, and other choices give qualitatively the same results.

## III. RESULTS AND DISCUSSION

We study the origin of the boson peak in 3D model glasses by molecular dynamics simulations. We focus on two different prototypical glass models with isotropic interactions; the 3D versions of the 2D models used in our previous study [36] (see Methods). The one model is an equimolar binary mixture of the atoms interacting via the inverse power-law potential ($\sim r^{-10}$; $r$: interparticle distance) (3DIPL) [62]. The other is the classical Kob-Andersen binary system with attractive long-range interactions (3DKA) [63]. Comparing these models helps us understand the role of interparticle attraction in glass vibrations. We analyze the vibrational properties of the low-temperature glass solids in their inherent states. We study samples of cuboid and cubic shapes but mainly show results from cubic samples, unless otherwise stated. We consider 3DIPL results in the main text and similar ones of 3DKA in the Appendix.

### A. The boson peak and dispersion relations

We first show the reduced VDOS of 3DIPL and 3DKA in Figs. 1(a) and 1(c), respectively. From its log-normal description [68], we can clearly see the boson peak and estimate $\omega_{\rm BP}$. The skewed asymmetric shape of the boson peak may be induced by the change in the spatial organization of the QLVs with frequency (see [36] and below). We also calculate the polarization-dependent dynamic structure factors $S_\alpha(q,\omega)$ ($\alpha = {\rm T}$ or L) [36,37,69]. They are analyzed by fitting the

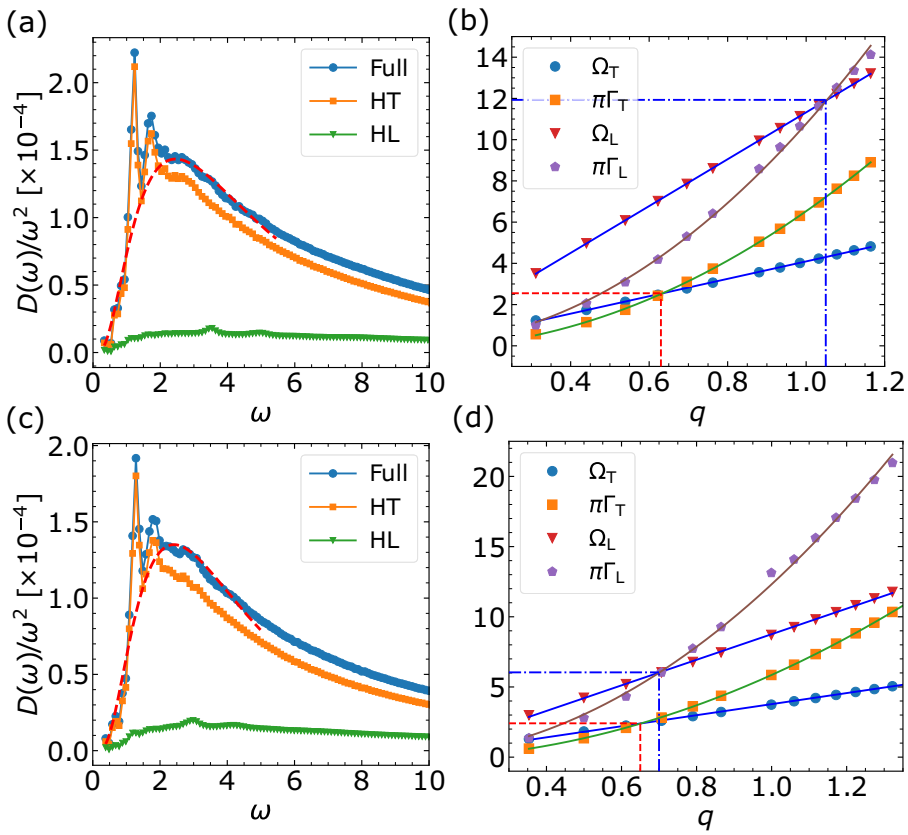


FIG. 1. The boson peak and dispersion relations of the two systems. (a) The reduced VDOS of 3DIPL from Hessian (Full) and its transverse (HT) and longitudinal components (HL). The low-frequency spectrum of Full is fitted by a log-normal function (red-dashed curve) while excluding the phononic peak contributions. The peak frequency gives $\omega_{\rm BP}$. (b) The dispersion relations of 3DIPL. The red-dashed lines mark the Ioffe-Regel wave number $q_{\rm IR}^{\rm T}$ and frequency $\omega_{\rm IR}^{\rm T}$ of the transverse phonons. The blue-dot-dashed lines give $q_{\rm IR}^{\rm L}$ and $\omega_{\rm IR}^{\rm L}$ of the longitudinal phonons. The solid lines are fits to $\Omega_\alpha \sim c_\alpha q$ and $\pi\Gamma_\alpha \sim \gamma_\alpha q^2$ ($\alpha \in \{{\rm T},{\rm L}\}$). (c) and (d) show the same quantities as in (a) and (b), respectively, for 3DKA.

TABLE I. Characteristic parameters of the two glass systems studied.

| Model | $\omega_{\rm BP}$ | $\omega_{\rm IR}^{\rm T}$ | $q_{\rm IR}^{\rm T}$ | $\omega_{\rm IR}^{\rm L}$ | $q_{\rm IR}^{\rm L}$ | $c_{\rm T}$ | $c_{\rm L}$ | $\gamma_{\rm T}$ | $\gamma_{\rm L}$ | $K$ | $G$ | $\omega_{\rm min,T}^{\rm phonon}$ | $\omega_{\rm min,L}^{\rm phonon}$ |
|---|---|---|---|---|---|---|---|---|---|---|---|---|---|
| 3DIPL | 2.46 | 2.55 | 0.63 | 11.93 | 1.05 | 4.23 | 11.36 | 6.66 | 10.65 | 88.46 | 14.08 | 1.18 | 3.50 |
| 3DKA | 2.41 | 2.41 | 0.65 | 6.04 | 0.70 | 3.94 | 9.11 | 6.01 | 12.36 | 65.31 | 17.85 | 1.23 | 2.87 |

damped harmonic oscillator (DHO) model,

$$S_\alpha(q,\omega) \propto \frac{\Omega_\alpha^2 \Gamma_\alpha}{\left(\omega^2 - \Omega_\alpha^2\right)^2 + \omega^2 \Gamma_\alpha^2}, \tag{15}$$

in which $\Omega_\alpha$ is the excitation frequency and $\Gamma_\alpha$ gives the sound attenuation rate. In Figs. 1(b) and 1(d), we show the dispersion relations for 3DIPL and 3DKA, respectively. In this low-$q$ range, $\Omega_\alpha$ is linear with $q$, and its slope gives the sound velocity $c_\alpha$. The estimated sound velocities are compared with $c_{\rm T} = \sqrt{G/\rho}$ and $c_{\rm L} = \sqrt{(K + 4G/3)/\rho}$, which are independently estimated from the macroscopic shear modulus $G$ and bulk modulus $K$ ($\rho$: number density). The minimal frequencies of transverse phonons ($\omega_{\rm min,T}^{\rm phonon}$) and longitudinal phonons ($\omega_{\rm min,L}^{\rm phonon}$) due to the finite box size are also measured accordingly. Note that the box length determines the minimum frequency of phonons propagating in a simulation box. On the other hand, $\pi\Gamma_\alpha$ obeys the quadratic law as $\gamma_\alpha q^2$, where $\gamma_\alpha$ is the damping coefficient. We note that our system size is too small to access the low-frequency Rayleigh damping regime [29,70]. The condition

$$\Omega_\alpha(q) = \pi\Gamma_\alpha(q) \tag{16}$$

gives the corresponding Ioffe-Regel limit frequency $\omega_{\rm IR}^\alpha$ and wave number $q_{\rm IR}^\alpha$ for transverse ($\alpha = {\rm T}$) and longitudinal ($\alpha = {\rm L}$) modes [71]. The values of these quantities are summarized in Table I.

The dispersion relations vividly show a remarkable difference between the two systems. In 3DIPL, $\omega_{\rm IR}^{\rm T}$ and $q_{\rm IR}^{\rm T}$ are quite different from $\omega_{\rm IR}^{\rm L}$ and $q_{\rm IR}^{\rm L}$, respectively. On the contrary, their differences are much smaller in 3DKA. This difference should result mainly from the much larger damping coefficient ratio $\gamma_{\rm L}/\gamma_{\rm T}$ for 3DKA than for 3DIPL. Their sound velocities and elastic properties are also different, but with less amount. For 3DKA with long-range attractions, the sample is more shear resistant and less compression tolerant. Therefore, we can conclude that these two systems have very different mechanical properties, indicating that the attractive interactions significantly affect the macroscopic mechanical properties of glasses. Nevertheless, their $\omega_{\rm BP}$ is very close to each other. More importantly, we can easily confirm that $\omega_{\rm BP} \approxeq \omega_{\rm IR}^{\rm T} < \omega_{\rm IR}^{\rm L}$ [37]. This indicates that the boson peak is closely related to the transverse modes, not the longitudinal ones. Above $\omega_{\rm BP}$, transverse phonons are strongly scattered and can no longer propagate, while longitudinal phonons can propagate normally.

### B. Longitudinal-transverse mode decomposition

To reveal the transverse and longitudinal modes in real space and characterize the atomic-scale features, we employ a volume matrix method developed by Beltukov *et al.* [67] (see Methods for the details). By definition, transverse modes do not involve volume change, whereas longitudinal modes do. Based on this feature, we decompose each eigenmode $\vec{u}$ into the transverse (T) component $\vec{u}_{\rm T}$ and longitudinal (L) component $\vec{u}_{\rm L}$: $\vec{u} = \vec{u}_{\rm T} + \vec{u}_{\rm L}$ and $\|\vec{u}\|^2 = \|\vec{u}_{\rm T}\|^2 + \|\vec{u}_{\rm L}\|^2 = 1.0$. A typical example of independent low-frequency multipolar QLM ($\omega < \omega_{\rm min,T}^{\rm phonon}$) and its T-L mode decompositions are shown in the Appendix (Fig. 6). Its key feature is the core with remarkable longitudinal components, i.e., volumetric vibrations (note that their $\omega \ll \omega_{\rm min,L}^{\rm phonon}$).

With this method, we decompose each eigenmode in the full frequency spectrum into transverse and longitudinal ones and calculate the reduced VDOS for the transverse modes $[D^{\rm T}(\omega)/\omega^2]$ and the longitudinal modes $[D^{\rm L}(\omega)/\omega^2]$. We show the results of 3DIPL and 3DKA in Figs. 1(a) and 1(c), respectively. Remarkably, the VDOS of each system is dominated by the transverse component. The longitudinal component has a much weaker intensity than the transverse one and the almost $\omega$-independent intensity, i.e., Debye behavior. Thus, we may conclude that the boson peak has a purely transverse nature, consistent with the above finding of $\omega_{\rm BP} \approxeq \omega_{\rm IR}^{\rm T}$.

Furthermore, we calculate the participation ratio PR and its transverse and longitudinal components for each vibration mode. We illustrate the frequency dependence of these PR's in the entire frequency range in Fig. 2. Figure 2(a) displays the full modes, showing general glassy solids' general characteristics. We can see that $\omega_{\rm BP}$ is higher than the phononic peak frequencies and lower than $\omega_{\rm IR}^{\rm L}$, but coincides with $\omega_{\rm IR}^{\rm T}$. More importantly, the transverse modes in Fig. 2(b) show features quite similar to the full modes, especially in the low-frequency range. In contrast, the longitudinal modes in Fig. 2(c) display features distinct from the full modes in the low-frequency range. The common features among the three modes are the PR plateau at intermediate frequencies and the "Anderson localization" at very high frequencies. All these features are pretty similar to the 2D glasses [36].

The first two obvious phononic peaks from the full modes [Fig. 2(a)] are the contribution of the transverse components. Significantly, the first phononic peak frequency in transverse modes [Fig. 2(b)] coincides with $\omega_{\rm min,T}^{\rm phonon}$ that is independently determined from the dispersion relations. The first phononic peak in longitudinal modes [Fig. 2(c)] also coincides with $\omega_{\rm min,L}^{\rm phonon}$. These results confirm the validity of our real-space mode decomposition, consistent with the usual reciprocal-space one. The relationship among these characteristic frequencies can be summarized as follows:

$$\omega_{\rm min,T}^{\rm phonon} < \omega_{\rm BP} \approxeq \omega_{\rm IR}^{\rm T} < \omega_{\rm min,L}^{\rm phonon} < \omega_{\rm IR}^{\rm L}. \tag{17}$$

Here we emphasize that $\omega_{\rm min,L}^{\rm phonon} > \omega_{\rm BP}$, and thus the boson peak is free from longitudinal phonons. The longitudinal component of $D(\omega)/\omega^2$ [see Figs. 1(a) and 1(c)] comes from

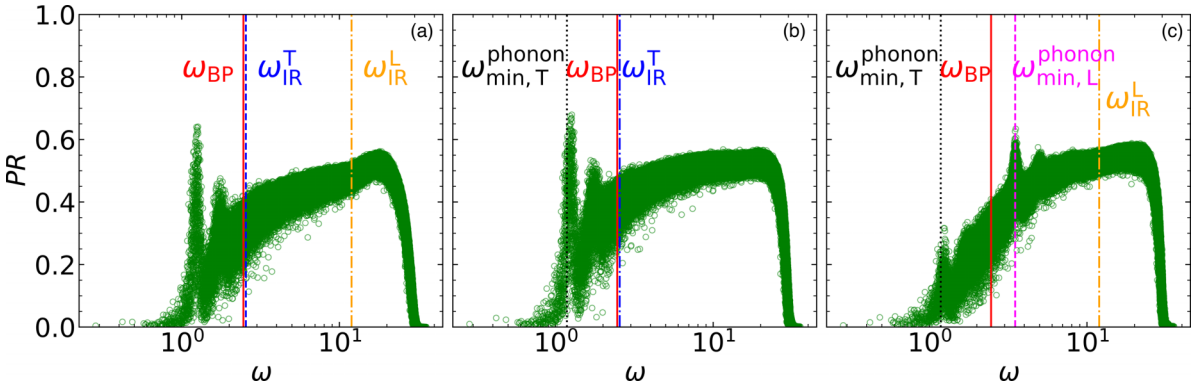


FIG. 2. Participation ratios and characteristic frequencies of 3DIPL. (a) All full eigenmodes. (b) The corresponding transverse modes. (c) The corresponding longitudinal modes. Here the transverse-longitudinal decomposition is made in real space [67] (see Appendix).

quasilocalized longitudinal vibrations, whose degree of delocalization (i.e., PR) increases with $\omega$ (see Fig. 2).

An additional interesting point is the coincidence of the lowest frequency peak of the longitudinal component in Fig. 2(c) with $\omega_{\mathrm{min,T}}^{\mathrm{phonon}}$ . This indicates the strong hybridization of the transverse phonons with a multipolar QLM, giving rise to the longitudinal component through their core's longitudinal vibrations. We can confirm that multipolar QLMs have longitudinal vibrations in their cores (see, e.g., Fig. 3). Thus, the absence of the boson peak in the longitudinal component of $D(\omega)/\omega^2$ in Figs. 1(a) and 1(c) indicates the negligible contribution of the longitudinal core vibrations of multipolar QLMs to the boson peak. We note that this finding can be made only through the T-L mode decomposition of the vibrational modes of glasses.

### C. $q$-dependent dynamical structure factors

Now, we focus on the nature of the vibrations responsible for the boson peak. To this end, we measure the dynamic structure factors in a much broader $q$ range, even above the pseudo-Brillouin zone boundary. We show typical results of these transverse and longitudinal dynamic structure factors in Fig. 4 for cuboid samples of 3DIPL (see also Fig. 7 in the Appendix). Only in this sample geometry can we access lower $q$. Similar results of the cubic samples for both systems are shown in the Appendix. We confirm the negligible effects of the sample shape and system size on the boson peak, elasticity, and dispersion relations (see the Appendix). Figures 4(a) and 4(b) show 1D and 2D plots of $S_{\mathrm{T}}(q,\omega)$, in which a subpeak around $\omega_{\mathrm{BP}}$ increases its intensity at a constant frequency with increasing $q$. This suggests that the "localized" transverse vibrations giving rise to this peak, which is characterized by the frequency and not by the wave number, is the origin of the boson peak. Similar to the 2D glasses [36], the full spectrum is well described by combining the DHO model for the phononic part and a log-normal function [68] for the nondispersive QLVs:

$$S_{\mathrm{T}}(q,\omega) \propto \frac{\Omega_{\mathrm{T}}^2\Gamma_{\mathrm{T}}}{\left(\omega^2-\Omega_{\mathrm{T}}^2\right)^2+\omega^2\Gamma_{\mathrm{T}}^2} + \frac{e^{-(\ln\omega-\mu)^2/2\sigma^2}}{\omega\sigma\sqrt{2\pi}}, \quad (18)$$

where the variables other than $\omega$ are fitting parameters. The individual contribution of these two functions to $S_{\mathrm{T}}(q,\omega)$ is demonstrated in Fig. 4(a). In contrast, such subpeak behavior is absent from $S_{\mathrm{L}}(q,\omega)$, as shown in Fig. 4(c). Instead, the full spectrum is well described by the sum of the Lorentzian function for the quasielastic component and the DHO model for longitudinal phonons

$$S_{\mathrm{L}}(q,\omega) \propto \frac{1}{\pi}\frac{\gamma}{\omega^2+\gamma^2} + \frac{\Omega_{\mathrm{L}}^2\Gamma_{\mathrm{L}}}{\left(\omega^2-\Omega_{\mathrm{L}}^2\right)^2+\omega^2\Gamma_{\mathrm{L}}^2}, \quad (19)$$

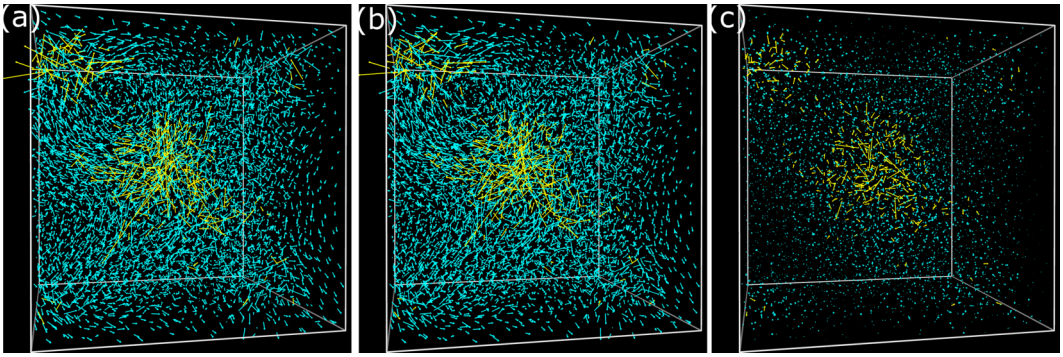


FIG. 3. Visualization of a low-frequency mode at $\omega_{\mathrm{min,T}}^{\mathrm{phonon}}$ of 3DIPL. (a) Full eigenmode field $\vec{u}$ with PR = 0.019. (b) The transverse component $\vec{u}_{\mathrm{T}}$ of (a) ($\|\vec{u}_{\mathrm{T}}\|^2 = 0.899$). (c) The longitudinal component $\vec{u}_{\mathrm{L}}$ of (a) ($\|\vec{u}_{\mathrm{L}}\|^2 = 0.101$). For comparison, the vectors of the atoms belonging to the longitudinal core are shown in yellow in (a)–(c).

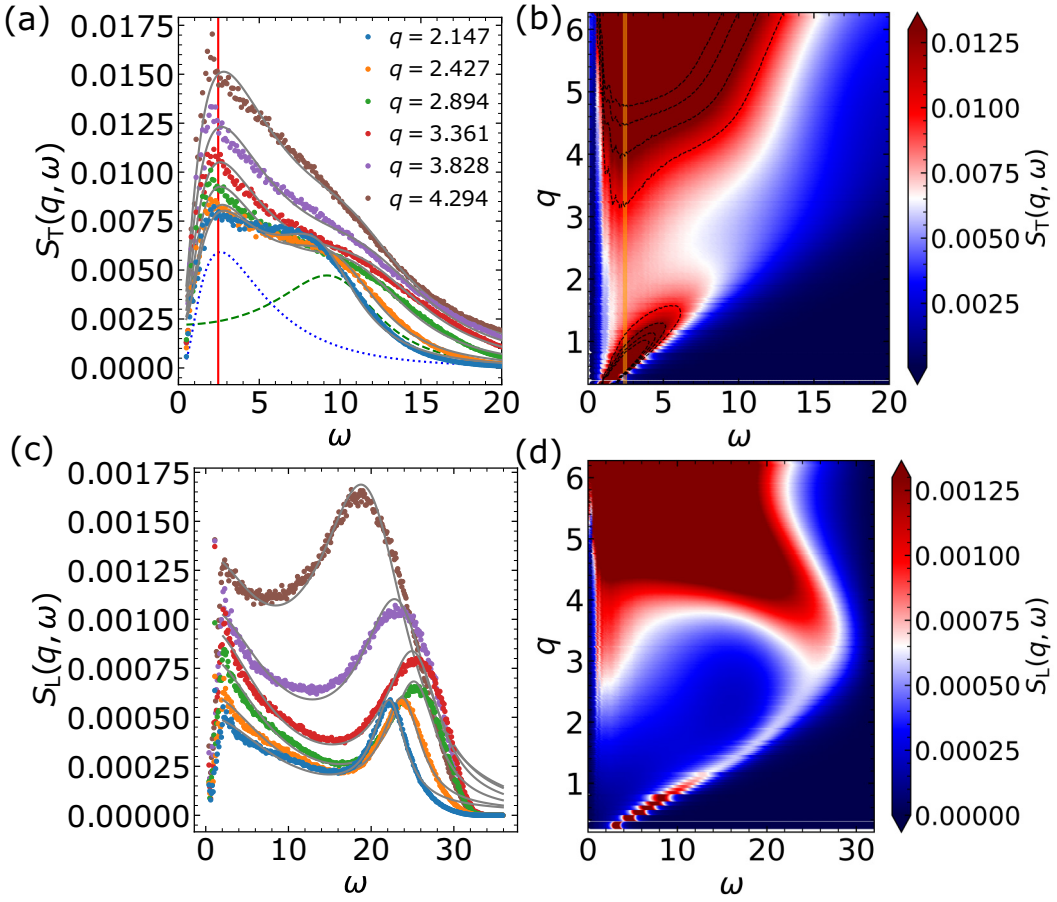


FIG. 4. Dynamic structure factors of the non-cubic-shape 3DIPL glasses. (a) and (b) are 1D and 2D plots of $S_T(q, \omega)$. The red and orange solid vertical lines in (a) and (b) indicate $\omega_{BP}$. The solid gray curves are fits to Eq. (18). The blue dotted and the purple dashed curves are the log-normal and phononic parts at $q = 2.427$ (a). (c) and (d) are 1D and 2D plots of $S_L(q, \omega)$. (c) shares the same legend as (a). The solid gray curves are fits to Eq. (19).

where the variables other than $\omega$ are fitting parameters. The steep decay from the quasi-elastic-component intensity at very low frequencies is due to the longitudinal phonons being absent. Examples of $S_\alpha(q, \omega)$ at lower $q$ range are shown in the Appendix (Fig. 7). These results suggest the emergence of the boson peak from the transverse QLVs in our systems.

### D. Spatial patterns of QLVs

Benefiting from the T-L mode decomposition, we calculate the atomic-scale transverse reduced VDOS $D_i^T(\omega_x)/\omega_x^2$ at different frequencies $\omega_x$ (see Methods). This strategy allows us to identify the spatial distribution of the atoms that have substantial contributions to $D_i^T(\omega_x)/\omega_x^2$, especially around $\omega_{BP}$. Here we consider the top 5% at each $\omega_x$ to compare the core features of these QLMs. We note that the results shown below are insensitive to how to select the most active particles. We find that the structure of the QLVs strongly depends on the frequency, as it should. At very low frequencies below the first sound mode, the QLVs exhibit multipolar structures with large cores [Figs. 5(a) and 3], reminiscent of multipolar QLMs. On the other hand, around $\omega_{BP}$, the QLVs show 1D stringlike structures [Fig. 5(b)] [47–49,72]. They become shorter strings and then almost single atoms with increasing the frequencies [Fig. 5(c)]. The gradual dying away of strings with $\omega$ is probably responsible for the log-normal asymmetric shape of the boson peak in Figs. 1(a) and 1(c). We note that the fact that the selection of the top 5% of particles yields multipolar and stringlike QLVs in an $\omega$-dependent manner is not just a coincidence but the inevitable consequence of (quasi-)localizations of the key vibrational modes. Furthermore, the string-length distribution shows the exponential decay [49], as found in 2D systems [36], another $d$-independent universal feature.

### E. Generality of our findings in 3D glass-forming systems with isotropic interactions

In the Appendix, we show the results for the 3DKA system to see the generality of our findings to a system with long-range attraction. As shown below, all the essential features are shared between the 3DIPL and 3DKA systems, suggesting the generality of our findings to glass-forming systems irrespective of the dimensionality (at least 2D and 3D) as long as the interaction potential is isotropic.

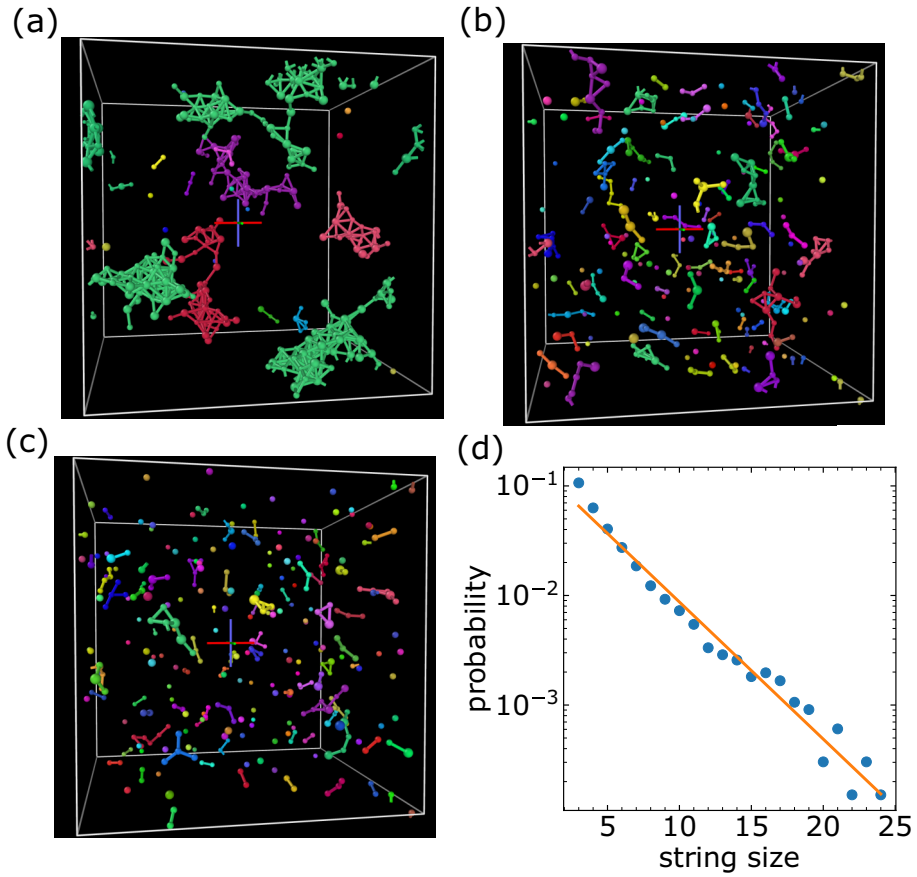


FIG. 5. Microscopic structural features of the QLMs of 3DIPL. For (a)–(c), the shown atoms are the top 5% of $D_i^{\mathrm{T}}(\omega_x)/\omega_x^2$ averaged over the frequency range of $\omega_x \pm 0.2$, where $\omega_x$ is 1.1, 2.5 ($\sim\omega_{\mathrm{BP}}$), and 4.0, respectively. The atoms are colored by cluster analysis. (d) The probability distribution of the string lengths around $\omega_{\mathrm{BP}}$. The cluster analysis and bond generation are based on the pair distances at the first minima of the partial pair correlation functions.

## IV. SUMMARY AND OUTLOOK

In summary, we unveil that the boson peak originates from stringlike transverse vibrations by simulating two popular glass models with isotropic interactions in three dimensions. These QLVs give rise to an additional peak at the boson peak frequency besides a phonon peak in the transverse dynamic structure factor at high $q$. The boson peak appears at the crossover frequency of transverse phonons from propagating to overdamped, i.e., at the transverse Ioffe-Regel limit. This is because when the frequency of the transverse phonon resonates with the frequency of the stringlike vibrations, its scattering cross section also resonantly increases. The atomic vibrations responsible for the boson peak show 1D stringlike structures in 3D space. These features we found in 3D glasses are the same as in 2D glasses, indicating the universal 1D nature of QLVs, independent of the spatial dimensionality $d$.

We also show that our findings are general to glass-forming systems with repulsive and attractive interactions irrespective of the dimensionality as long as the interaction is isotropic (see Ref. [36] for 2D systems and the Appendix for the 3DKA with attractive interaction). It suggests that amorphous "defects" responsible for high-frequency local vibrations come from the same structural feature for both repulsive and attractive systems. A similar conclusion has recently been derived for the slow structural relaxation of glass-forming systems [73,74]. These facts imply that the dynamics of glass-forming liquids and their glass state from the slowest to fastest may be described based on the common structural feature (or, order parameter [75]). This point needs further studies.

Our study also indicates the two types of quasilocalized vibrations in glasses: Multipolar QLMs and stringlike QLVs. The former has been considered the origin of the boson peak for a long time, e.g., in the soft potential model. However, our results have indicated, at least apparently, that the latter is responsible for the boson peak. Multipolar QLMs have longitudinal vibrations in their cores at least at low frequencies [see Fig. 3(c)] and accompany space-spanning power-law-decaying strain fields whose angular symmetry and power-law exponent depend on $d$ (see, e.g., [10] for review). On the other hand, stringlike QLVs, coherent vibrations of a chain of particles weakly bound to the surroundings, have a purely transverse and 1D nature independent of $d$. These unique features of stringlike QLVs not only indicate the $d$-independent universal origin of the boson peak (at least for $d = 2$ and 3 with practical importance) but also explain the purely transverse nature of the boson peak in glasses with isotropic interactions. We speculate that because of the locality and transverse (volume-inactive) nature, such chainlike vibrations can be most efficiently and abundantly excited in dense disordered systems. The origin of stringlike QLVs, including the relationship with multipolar QLMs, remains a challenging problem due to their hybridization with phonons and thus needs further study.

Here, we also mention the phonon scattering mechanism. The coincidence of the boson peak and the Ioffe-Regel limit of transverse phonons and the wave-number-independent peak frequency of the localized peak in the transverse dynamic structure factor [Fig. 4(b)] seems to suggest the frequency-

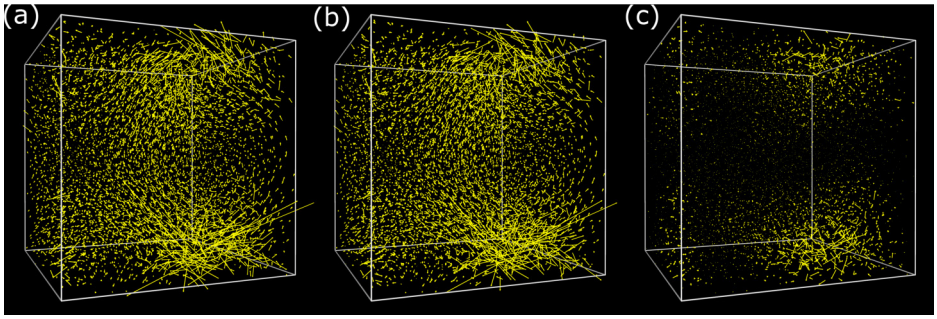


FIG. 6. Visualization of a low-frequency multipolar QLM of 3DIPL. (a) Full eigenmode field $\vec{u}$ at the frequency $\omega = 0.947$ and the participation ratio PR $= 0.012$. (b) The transverse component $\vec{u}_{\rm T}$ of (a) ($\|\vec{u}_{\rm T}\|^2 = 0.887$). (c) The longitudinal component $\vec{u}_{\rm L}$ of (a) ($\|\vec{u}_{\rm L}\|^2 = 0.113$). Other modes, including those from 3DKA, show similar features.

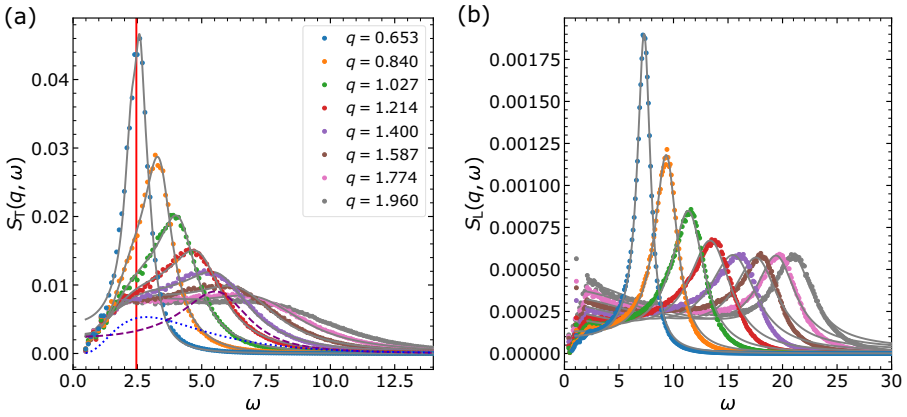


FIG. 7. Dynamical structure factors of noncubic shape 3DIPL. These figures supplement Fig. 4 in the main text to show the results in a lower $q$ range. (a) Transverse $S(q,\omega)$. The solid gray lines are fits to Eq. (18) in the main text. The blue dotted and the purple dashed curves are the log-normal and phononic parts, respectively, at $q = 1.400$. (b) Longitudinal $S(q,\omega)$. The solid gray lines are fits to Eq. (19) in the main text.

resonant scattering of transverse phonons by quasilocalized transverse modes rather than the scattering due to spatial elastic heterogeneity. These points need further study to be clarified.

In this study, we focus on 3D systems with isotropic interactions in which the transverse modes are not directly coupled with the longitudinal ones. Thus, we find the dominant contribution of the boson peak from transverse modes. However, this situation may depend on the structural characteristics of glassy materials controlled by the underlying interatomic potentials. The question of how the transverse-longitudinal coupling affects the boson peak of tetrahedral glasses, such as silica [69], silicon, and water, remains an interesting question for future study. Experimental access to longitudinal and transverse dynamic structure factors over a broad $q$-$\omega$ range is highly desirable.

## ACKNOWLEDGMENTS

This work was partially supported by Grants-in-Aid for Specially Promoted Research (JP20H05619) and Scientific Research (A) (JP18H03675) from the Japan Society of the Promotion of Science (JSPS). Y.C.H. is grateful for the financial support from a JSPS International Research fellowship (JP19F19021).

## APPENDIX

In this Appendix, we show additional results of 3DIPL (Figs. 6–11). We calculated the transverse and longitudinal dynamical structure factors at the ultrawide frequency and wave-number ranges for different system sizes ($N = 6750$ vs $N = 1000$) and different simulation box shapes (cubic vs noncubic). They all show consistent behaviors, which demonstrates the robustness of our analysis.

Furthermore, we present the results of 3DKA with long-range Lennard-Jones interaction. We performed comprehensive analyses similar to 3DKA (Figs. 12–15). These results verify that the origin of the boson peak in glasses is the same between 3D glass-forming systems with repulsive and attractive interactions as long as the interactions are isotropic.

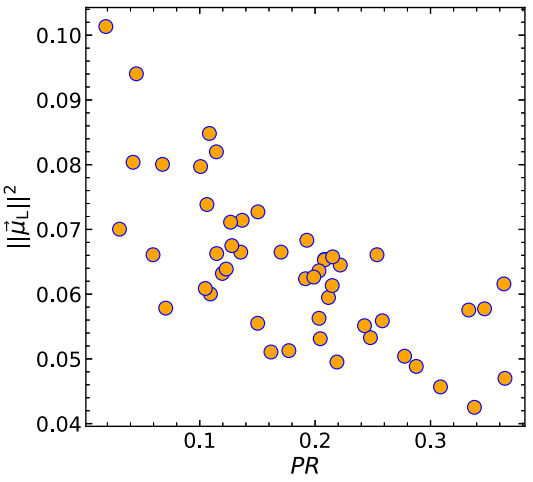


FIG. 8. Relationship between the longitudinal component $\|\vec{u}_{\rm L}\|^2$ and the participation ratio PR for vibration modes at $\omega^{\rm phonon}_{\rm min,T}$ of 3DIPL. We pick up the vibration mode with the largest $\|\vec{u}_{\rm L}\|^2$ for each sample. In general, they are negatively correlated. The larger PR of the mode indicates the higher similarity to a pure transverse phonon. Thus, the coupling strength shall be weaker for smaller $\|\vec{u}_{\rm L}\|^2$.

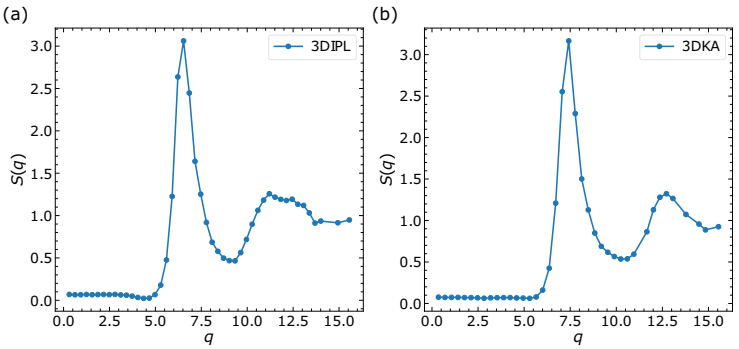


FIG. 9. The static structure factors of 3DIPL (a) and 3DKA (b), respectively.

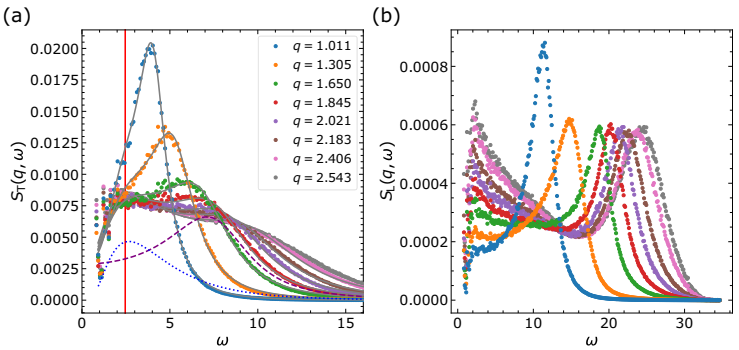


FIG. 10. Dynamical structure factors of 3DIPL with $N = 1000$ and cubic shape. (a) Transverse modes. The solid red line represents $\omega_{\mathrm{BP}}$. The solid gray lines in (a) are fits to Eq. (18) in the main text. The blue dotted and purple dashed lines are the log-normal and phononic parts for $q = 1.845$. (b) Longitudinal modes at the same $q$ as in (a).

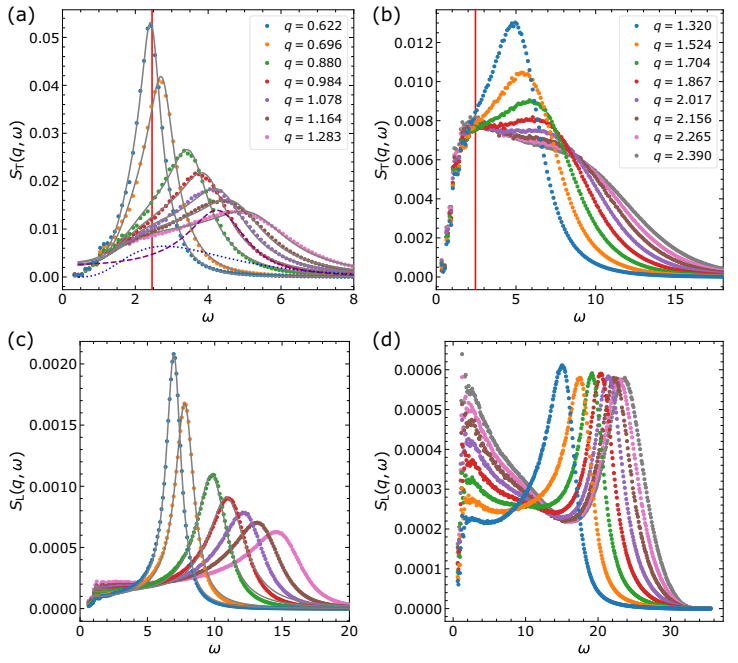


FIG. 11. Dynamical structure factors of 3DIPL with $N = 6750$ and cubic shape. (a) and (b) are for transverse modes. The solid red line represents $\omega_{\mathrm{BP}}$. The solid gray lines in (a) are fits to Eq. (18) in the main text. The blue dotted line and the purple dashed line are the log-normal and the phononic parts for $q = 1.078$. (c) and (d) are for longitudinal modes. (c) and (d) share the legend with (a) and (b), respectively. The solid gray lines in (c) are fits to Eq. (19) in the main text.

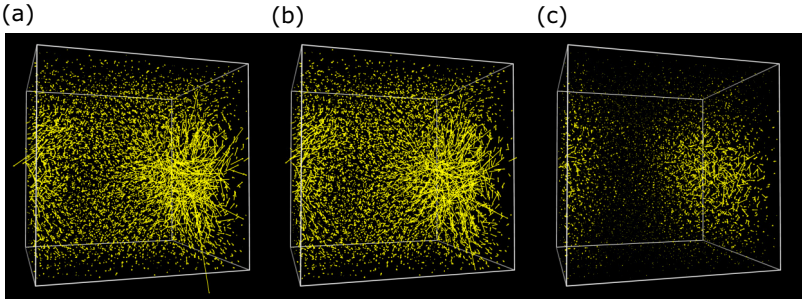


FIG. 12. Visualization of a low-frequency multipolar QLM of 3DKA. (a) Full eigenmode field $\vec{u}$ at the frequency $\omega = 0.908$ and the participation ratio $\mathrm{PR} = 0.002$. (b) The transverse component $\vec{u}_{\mathrm{T}}$ of (a) ($\|\vec{u}_{\mathrm{T}}\|^2 = 0.841$). (c) The longitudinal component $\vec{u}_{\mathrm{L}}$ of (a) ($\|\vec{u}_{\mathrm{L}}\|^2 = 0.159$).

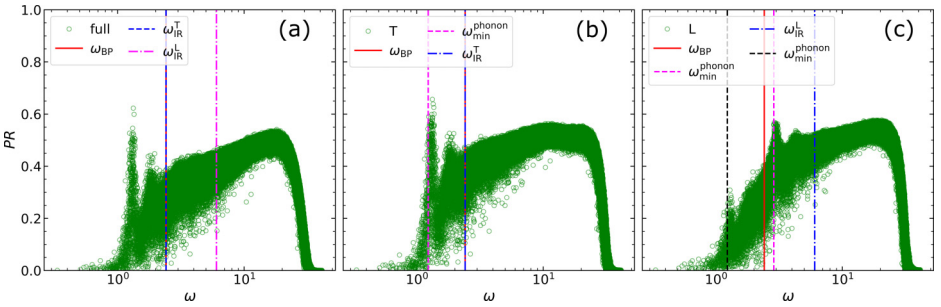


FIG. 13. Participation ratios and characteristic frequencies of 3DKA. (a) All full eigenmodes. (b) The corresponding transverse modes. (c) The corresponding longitudinal modes.

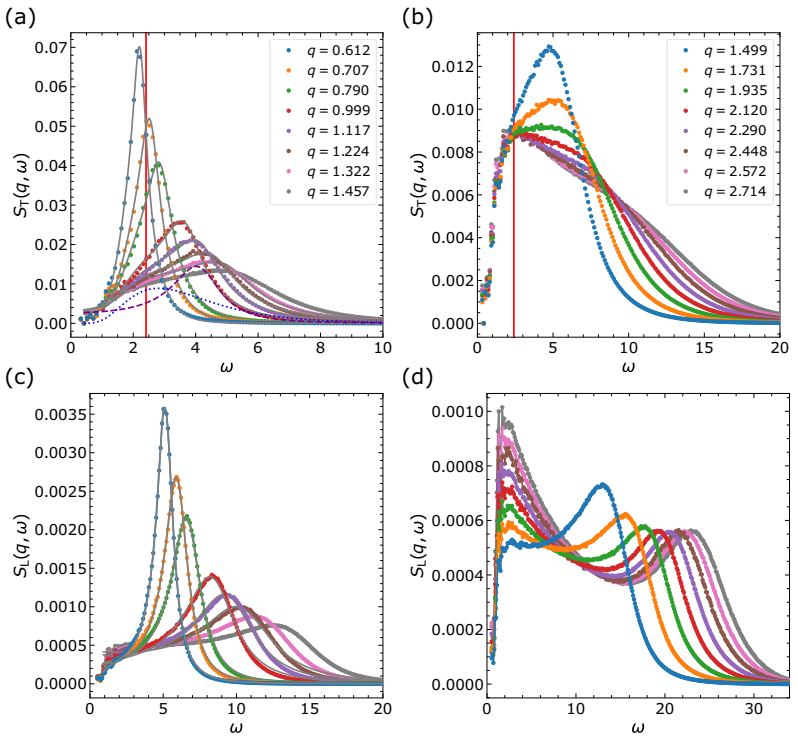


FIG. 14. Dynamical structure factors of 3DKA. (a) and (b) are for transverse modes. The solid red line represents $\omega_{\mathrm{BP}}$. The solid gray lines in (a) are fits to Eq. (18) in the main text. The blue dotted and purple dashed lines are the log-normal and phononic parts for $q = 1.117$. (c) and (d) are for longitudinal modes. (c) and (d) share the legend with (a) and (b), respectively. The solid gray lines in (c) are fits to Eq. (19) in the main text.

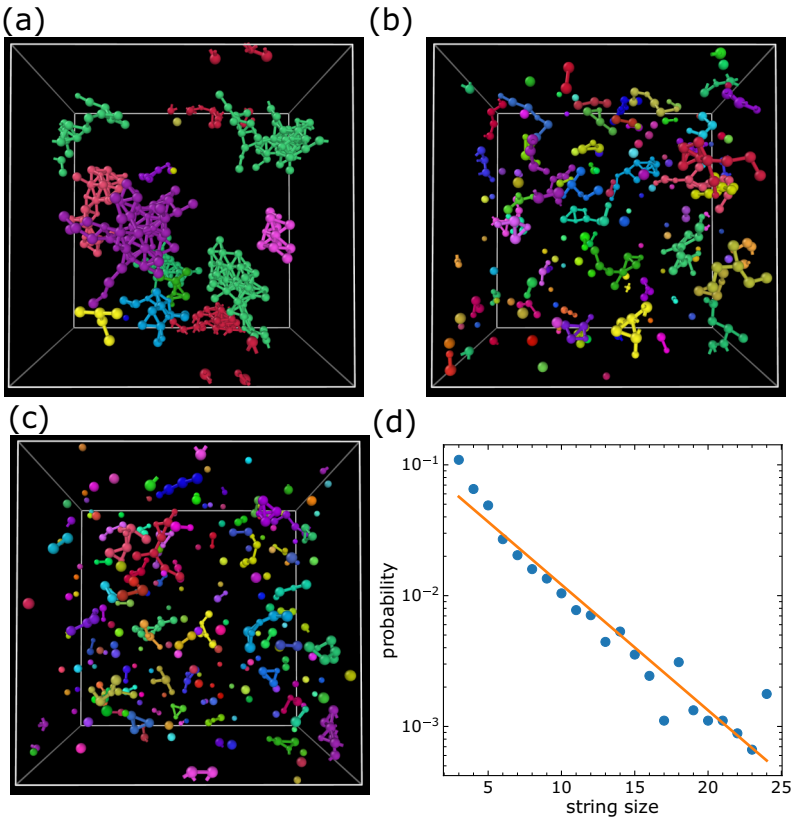


FIG. 15. Atomic-scale features of the quasilocalized modes of 3DKA. For (a), (b), and (c), the shown atoms are the top 5% of $D^i_{\mathrm{T}}(\omega_x)/\omega_x^2$, where $\omega_x$ is 1.1, 2.4 ($\sim\omega_{\mathrm{BP}}$), and 4.0, respectively. (d) The probability distribution of the string lengths around $\omega_{\mathrm{BP}}$. The bonds are generated based on the first minima of the partial pair correlation functions.


[1] R. C. Zeller and R. O. Pohl, Thermal conductivity and specific heat of noncrystalline solids, Phys. Rev. B **4**, 2029 (1971).

[2] *Amorphous Solids: Low-Temperature Properties*, edited by W. A. Phillips (Springer-Verlag, Berlin, 1981).

[3] S. Alexander, Amorphous solids: their structure, lattice dynamics and elasticity, Phys. Rep. **296**, 65 (1998).

[4] R. S. Krishnan, The scattering of light in fused quartz and its Raman spectrum, in *Proceedings of the Indian Academy of Sciences, Section A* (Indian Academy of Sciences, 1953), Vol. 37, pp. 377–384.

[5] J. Jäckle, On the ultrasonic attenuation in glasses at low temperatures, Z. Phys. **257**, 212 (1972).

[6] U. Buchenau, M. Prager, N. Nücker, A. J. Dianoux, N. Ahmad, and W. A. Phillips, Low-frequency modes in vitreous silica, Phys. Rev. B **34**, 5665 (1986).

[7] V. K. Malinovsky and A. P. Sokolov, The nature of boson peak in Raman scattering in glasses, Solid State Commun. **57**, 757 (1986).

[8] T. Nakayama, Boson peak and terahertz frequency dynamics of vitreous silica, Rep. Prog. Phys. **65**, 1195 (2002).

[9] P. B. Allen, J. L. Feldman, J. Fabian, and F. Wooten, Diffusons, locons and propagons: Character of atomic vibrations in amorphous Si, Philos. Mag. B **79**, 1715 (1999).

[10] E. Lerner and E. Bouchbinder, Low-energy quasilocalized excitations in structural glasses, J. Chem. Phys. **155**, 200901 (2021).

[11] S. R. Elliott, A unified model for the low-energy vibrational behaviour of amorphous solids, Europhys. Lett. **19**, 201 (1992).

[12] W. Schirmacher, Thermal conductivity of glassy materials and the "boson peak", Europhys. Lett. **73**, 892 (2006).

[13] W. Schirmacher, G. Ruocco, and T. Scopigno, Acoustic Attenuation in Glasses and its Relation with the Boson Peak, Phys. Rev. Lett. **98**, 025501 (2007).

[14] W. Schirmacher, G. Ruocco, and V. Mazzone, Heterogeneous Viscoelasticity: A Combined Theory of Dynamic and Elastic Heterogeneity, Phys. Rev. Lett. **115**, 015901 (2015).

[15] F. Leonforte, A. Tanguy, J. P. Wittmer, and J. L. Barrat, Inhomogeneous Elastic Response of Silica Glass, Phys. Rev. Lett. **97**, 055501 (2006).

[16] Y. M. Galperin, V. G. Karpov, and V. I. Kozub, Localized states in glasses, Adv. Phys. **38**, 669 (1989).

[17] U. Buchenau, Y. M. Galperin, V. L. Gurevich, and H. R. Schober, Anharmonic potentials and vibrational localization in glasses, Phys. Rev. B **43**, 5039 (1991).

[18] M. I. Klinger and A. M. Kosevich, Soft-mode dynamics model of boson peak and high frequency sound in glasses: "inelastic" Ioffe-Regel crossover and strong hybridization of excitations, Phys. Lett. A **295**, 311 (2002).

[19] V. L. Gurevich, D. A. Parshin, and H. R. Schober, Anharmonicity, vibrational instability, and the boson peak in glasses, Phys. Rev. B **67**, 094203 (2003).

[20] D. A. Parshin, H. R. Schober, and V. L. Gurevich, Vibrational instability, two-level systems, and the boson peak in glasses, Phys. Rev. B **76**, 064206 (2007).

[21] W. Götze and M. R. Mayr, Evolution of vibrational excitations in glassy systems, Phys. Rev. E **61**, 587 (2000).

[22] T. Grigera, V. Martín-Mayor, G. Parisi, and P. Verrocchio, Phonon interpretation of the 'boson peak' in supercooled liquids, Nature (London) **422**, 289 (2003).

[23] M. Baggioli and A. Zaccone, Universal Origin of Boson Peak Vibrational Anomalies in Ordered Crystals and in Amorphous Materials, Phys. Rev. Lett. **122**, 145501 (2019).

[24] S. N. Taraskin, Y. L. Loh, G. Natarajan, and S. R. Elliott, Origin of the Boson Peak in Systems with Lattice Disorder, Phys. Rev. Lett. **86**, 1255 (2001).

[25] A. I. Chumakov, G. Monaco, A. Monaco, W. A. Crichton, A. Bosak, R. Rüffer, A. Meyer, F. Kargl, L. Comez, D. Fioretto *et al.*, Equivalence of the Boson Peak in Glasses to the Transverse Acoustic van Hove Singularity in Crystals, Phys. Rev. Lett. **106**, 225501 (2011).

[26] H. R. Schober, Quasi-localized vibrations and phonon damping in glasses, J. Non-Cryst. Solids **357**, 501 (2011).

[27] H. R. Schober and G. Ruocco, Size effects and quasilocalized vibrations, Philos. Mag. **84**, 1361 (2004).

[28] M. Shimada, H. Mizuno, M. Wyart, and A. Ikeda, Spatial structure of quasilocalized vibrations in nearly jammed amorphous solids, Phys. Rev. E **98**, 060901(R) (2018).

[29] L. Wang, A. Ninarello, P. Guan, L. Berthier, G. Szamel, and E. Flenner, Low-frequency vibrational modes of stable glasses, Nat. Commun. **10**, 26 (2019).

[30] S. Kojima, *Low Energy Excitations in Borate Glass*, Characteristics and Applications of Boron, edited by C. Wongchoosuk (IntechOpen, London, 2022).

[31] H. R. Schober and C. Oligschleger, Low-frequency vibrations in a model glass, Phys. Rev. B **53**, 11469 (1996).

[32] D. Richard, G. Kapteijns, J. A. Giannini, M. L. Manning, and E. Lerner, Simple and Broadly Applicable Definition of Shear Transformation Zones, Phys. Rev. Lett. **126**, 015501 (2021).

[33] D. Richard, K. González-López, G. Kapteijns, R. Pater, T. Vaknin, E. Bouchbinder, and E. Lerner, Universality of the Nonphononic Vibrational Spectrum across Different Classes of Computer Glasses, Phys. Rev. Lett. **125**, 085502 (2020).

[34] S. Bonfanti, R. Guerra, C. Mondal, I. Procaccia, and S. Zapperi, Universal Low-Frequency Vibrational Modes in Silica Glasses, Phys. Rev. Lett. **125**, 085501 (2020).

[35] H. Mizuno, H. Shiba, and A. Ikeda, Continuum limit of the vibrational properties of amorphous solids, Proc. Natl. Acad. Sci. USA **114**, E9767 (2017).

[36] Y.-C. Hu and H. Tanaka, Origin of the boson peak in amorphous solids, Nat. Phys. **18**, 669 (2022).

[37] H. Shintani and H. Tanaka, Universal link between the boson peak and transverse phonons in glass, Nat. Mater. **7**, 870 (2008).

[38] T. Scopigno, J. B. Suck, R. Angelini, F. Albergamo, and G. Ruocco, High-Frequency Dynamics in Metallic Glasses, Phys. Rev. Lett. **96**, 135501 (2006).

[39] H. Mizuno, S. Mossa, and J.-L. Barrat, Acoustic excitations and elastic heterogeneities in disordered solids, Proc. Natl. Acad. Sci. USA **111**, 11949 (2014).

[40] G. Monaco and V. M. Giordano, Breakdown of the Debye approximation for the acoustic modes with nanometric wavelengths in glasses, Proc. Natl. Acad. Sci. USA **106**, 3659 (2009).

[41] G. Monaco and S. Mossa, Anomalous properties of the acoustic excitations in glasses on the mesoscopic length scale, Proc. Natl. Acad. Sci. USA **106**, 16907 (2009).

[42] A. P. Sokolov, R. Calemczuk, B. Salce, A. Kisliuk, D. Quitmann, and E. Duval, Low-Temperature Anomalies in Strong and Fragile Glass Formers, Phys. Rev. Lett. **78**, 2405 (1997).

[43] E. Duval, T. Deschamps, and L. Saviot, Poisson ratio and excess low-frequency vibrational states in glasses, J. Chem. Phys. **139**, 064506 (2013).

[44] V. N. Novikov, Spectrum of low-energy (2–10 meV) vibrational excitations of glasses in a disclination model, Pis'ma Zh. Eksp. Teor. Fiz. **51**, 65 (1990) [JETP Lett. **51** (1990).

[45] H. R. Schober, Soft phonons in glasses, Phys. A (Amsterdam, Neth.) **201**, 14 (1993).

[46] J. Hafner and M. Krajci, Propagating and localized vibrational modes in Ni-Zr glasses, J. Phys.: Condens. Matter **6**, 4631 (1994).

[47] H. Zhang and J. F. Douglas, Glassy interfacial dynamics of Ni nanoparticles: Part II. Discrete breathers as an explanation of two-level energy fluctuations, Soft Matter **9**, 1266 (2013).

[48] E. Bianchi, V. M. Giordano, and F. Lund, Elastic anomalies in glasses: Elastic string theory understanding of the cases of glycerol and silica, Phys. Rev. B **101**, 174311 (2020).

[49] H. Zhang, X. Wang, H.-B. Yu, and J. F. Douglas, Fast dynamics in a model metallic glass-forming material, J. Chem. Phys. **154**, 084505 (2021).

[50] H. Shiba, Y. Yamada, T. Kawasaki, and K. Kim, Unveiling Dimensionality Dependence of Glassy Dynamics: 2D Infinite Fluctuation Eclipses Inherent Structural Relaxation, Phys. Rev. Lett. **117**, 245701 (2016).

[51] S. Vivek, C. P. Kelleher, P. M. Chaikin, and E. R. Weeks, Long-wavelength fluctuations and the glass transition in two dimensions and three dimensions, Proc. Natl. Acad. Sci. USA **114**, 1850 (2017).

[52] B. Illing, S. Fritschi, H. Kaiser, C. L. Klix, G. Maret, and P. Keim, Mermin-Wagner fluctuations in 2D amorphous solids, Proc. Natl. Acad. Sci. USA **114**, 1856 (2017).

[53] G. Parisi and F. Zamponi, Mean-field theory of hard sphere glasses and jamming, Rev. Mod. Phys. **82**, 789 (2010).

[54] G. Biroli and J.-P. Bouchaud, The random first-order transition theory of glasses: A critical assessment, in *Structural Glasses and Supercooled Liquids* (Wiley Online Library, 2012), Chap. 2, pp. 31.

[55] T. R. Kirkpatrick and D. Thirumalai, *Colloquium*: Random first order transition theory concepts in biology and physics, Rev. Mod. Phys. **87**, 183 (2015).

[56] A. Lemaître, Tensorial analysis of Eshelby stresses in 3D supercooled liquids, J. Chem. Phys. **143**, 164515 (2015).

[57] A. Lemaître, Stress correlations in glasses, J. Chem. Phys. **149**, 104107 (2018).

[58] E. DeGiuli, Field Theory for Amorphous Solids, Phys. Rev. Lett. **121**, 118001 (2018).

[59] E. De Giuli, Renormalization of elastic quadrupoles in amorphous solids, Phys. Rev. E **101**, 043002 (2020).

[60] A. Lemaître, Stress hyperuniformity and transient oscillatory-exponential correlation decay as signatures of strength vs fragility in glasses, J. Chem. Phys. **155**, 194501 (2021).

[61] L. Wang, G. Szamel, and E. Flenner, Low-Frequency Excess Vibrational Modes in Two-Dimensional Glasses, Phys. Rev. Lett. **127**, 248001 (2021).

[62] E. Lerner and E. Bouchbinder, A characteristic energy scale in glasses, J. Chem. Phys. **148**, 214502 (2018).

[63] W. Kob and H. C. Andersen, Testing mode-coupling theory for a supercooled binary Lennard-Jones mixture. II. Intermediate scattering function and dynamic susceptibility, Phys. Rev. E **52**, 4134 (1995).

[64] R. J. Bell and P. Dean, Atomic vibrations in vitreous silica, Discuss. Faraday Soc. **50**, 55 (1970).

[65] F. H. Stillinger and T. A. Weber, Hidden structure in liquids, Phys. Rev. A **25**, 978 (1982).

[66] V. Mazzacurati, G. Ruocco, and M. Sampoli, Low-frequency atomic motion in a model glass, Europhys. Lett. **34**, 681 (1996).

[67] Y. M. Beltukov, C. Fusco, A. Tanguy, and D. A. Parshin, Transverse and longitudinal vibrations in amorphous silicon, J. Phys.: Conf. Ser. **661**, 012056 (2015).

[68] V. K. Malinovsky, V. N. Novikov, and A. P. Sokolov, Log-normal spectrum of low-energy vibrational excitations in glasses, Phys. Lett. A **153**, 63 (1991).

[69] J. Horbach, W. Kob, and K. Binder, High frequency sound and the boson peak in amorphous silica, Eur. Phys. J. B **19**, 531 (2001).

[70] S. Gelin, H. Tanaka, and A. Lemaître, Anomalous phonon scattering and elastic correlations in amorphous solids, Nat. Mater. **15**, 1177 (2016).

[71] A. F. Ioffe and A. R. Regel, Non-crystalline, amorphous, and liquid electronic semiconductors, Prog. Semicond. **4**, 237 (1960).

[72] B. A. Pazmiño Betancourt, F. W. Starr, and J. F. Douglas, String-like collective motion in the $\alpha$- and $\beta$-relaxation of a coarse-grained polymer melt, J. Chem. Phys. **148**, 104508 (2018).

[73] H. Tong, S. Sengupta, and H. Tanaka, Emergent solidity of amorphous materials as a consequence of mechanical self-organisation, Nat. Commun. **11**, 4863 (2020).

[74] H. Tong and H. Tanaka, Role of Attractive Interactions in Structure Ordering and Dynamics of Glass-Forming Liquids, Phys. Rev. Lett. **124**, 225501 (2020).

[75] H. Tanaka, H. Tong, R. Shi, and J. Russo, Revealing key structural features hidden in liquids and glasses, Nat. Rev. Phys. **1**, 333 (2019).